Design of Virtual Impedance Control Loop using the Complex Frequency Approach

Dionysios Moutevelis*, Javier Roldán-Pérez*, Milan Prodanovic*, and Federico Milano†
* IMDEA Energy, Madrid, Spain † University College Dublin, Dublin, Ireland
dionysios.moutevelis@imdea.org, javier.roldan@imdea.org, milan.prodanovic@imdea.org, federico.milano@ucd.ie

***Abstract*—In this paper the dynamic response of the virtual impedance control loop for power electronic converters is studied using the recently proposed concept of *complex frequency*. This quantity captures bus frequency variations due to changes in both the phase angle and the amplitude of the voltage and current. The paper derives analytically the link between complex power and complex frequency, allowing the incorporation of the virtual impedance control equations. First, the impact of the virtual impedance control on the complex frequency is considered independently of other control loops by simplifying the overall control structure. Then, the equations are generalised to include the interaction of the virtual impedance with a proportional-integral voltage controller. The paper shows that the proposed theoretical formulation allows identifying the dynamic effect of the virtual impedance and simplifies its design. These features are demonstrated by using simulations based on a modified version of the WSCC 9-bus system.**

***Index Terms*—Complex frequency, virtual impedance, converter control, voltage source converter.**

I. Introduction

A. Motivations

The output impedance has been identified as a critical parameter for the operation and stability of Voltage Source Converters (VSCs) [1]. A prominent way for shaping this impedance is through the Virtual Impedance (VI) control technique [2]. This method consists of emulating the operation of an impedance inside the converter control and avoids the costly manipulation of the converter hardware. Several implementations and design methods have been proposed in the literature [3, 4]. Although the operation of the VI loop and its design trade-offs have been intensely studied, the impact of VI parameters on the local frequency of the converter bus has not been discussed so far. In this paper, the recently proposed concept of Complex Frequency (CF) [5] is utilised to establish the analytical relationship between the VI control parameters and the local frequency of the converter connection bus.

B. Literature Review

VI controllers were originally implemented to improve power sharing in ac microgrids [6]. Then, their application has been extended to dc microgrids [7]. Other applications of these controllers include fast current limiting during transient conditions [8] and harmonic mitigation [9]. A critical property of VIs is their ability to improve power-sharing and stability margins when multiple grid-forming converters operate in parallel [4, 10]. This property has led to VIs being incorporated as part of grid-forming, cascaded control configurations [11].

The definition and estimation of the local frequency at the buses of a power system has been a relevant research topic, particularly during transient conditions [12]. In [13], a formula to estimate the frequency at the buses of a lossless power system was proposed. In [5], the definition of system frequency was expanded to a complex quantity, capturing frequency variations caused both from the change of voltage phase angle but also of voltage magnitude. By using CF, the assumption of a lossless system was dropped and an analytical link between the complex power injection at a bus, the rate of change of said power and the bus frequency was derived. From then on, CF was used to provide a taxonomy of power converter control schemes, including grid-following and grid-forming control structures [14]. The contribution and effect of VI in these control schemes was, though, omitted. In recent works, CF was used to introduce the concepts of complex synchronization and complex droop [15, 16]. Lastly, in [17], the concept of geometric frequency was proposed, of which the CF is a special case in two dimensions.

C. Contributions

In this paper, the novel quantity of CF is used to analytically derive the effect of the VI control loop at the frequency of the converter connection bus. The operation of the controller is assessed firstly independently and then also as a part of a complete, grid-forming control structure. The paper shows that the proposed theoretical formulation allows the separation of the VI effects from the rest of the control system and simplifies the selection of its control parameters. The theoretical contributions are validated by using simulations that include a grid-forming VSC and a realistic grid benchmark.

D. Paper Organization

The rest of the paper is organized as follows. In Section II, the VSC connection to the ac bus is explained and the block diagrams of the controllers studied in this work are presented. In Section III, some preliminary formulations regarding the CF are given. Then, in Section IV, the above formulations are utilised to derive analytically the link between VI parameters and the CF. A case study that validates the theoretical results is presented in Section V, providing guidelines in selecting the VI parameters. Finally, Section VI draws conclusions and outlines future work.

This work is partly supported by the Community of Madrid, research project PROMINT-CM (P2018/EMT4366) and Juan de la Cierva Incorporación program (IJC2019-042342-I) from the Spanish Government by funding D. Moutevelis, J. Roldán-Pérez, and M. Prodanovic and by the Sustainable Energy Authority of Ireland (SEAI) and the European Commission by funding F. Milano under projects FRESLIPS, Grant No. RDD/00681 and edgeFLEX, Grant No. 883710, respectively.

II. System and control overview

Figure 1 shows an overview of the VSC connection configuration and control, as studied in this work. The converter is connected to bus h of a larger power system through an LC filter. The dc part is represented with an ideal voltage source of voltage $v_{\rm dc}$. The controller consists of an outer voltage controller, a VI loop and two PI-based, cascaded voltage and current inner controllers. For the theoretical derivations presented in this work, ideal synchronization between the converter variables and the grid voltage is assumed. The reader is referred to [14] for understanding the effect of various synchronization mechanisms on the complex frequency of the connection bus. The VI loop and its interaction with the voltage controllers are the main focus of this work.

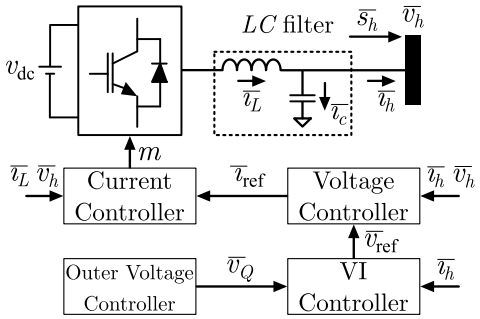

Fig. 1. VSC connection configuration and control overview.

Figure 2 shows the control scheme of the VI controller used throughout this work. Its implementation is based on the quasi-stationary approach, in which only the fundamental frequency is used for the reactance part [2]. This option is often preferred in practical applications to avoid high-frequency noise amplification via the emulation of the impedance across the full frequency spectrum [4, 18].

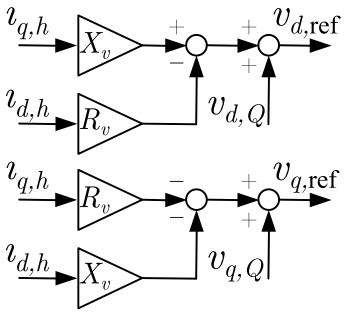

Fig. 2. Control scheme of VI control loop.

Figure 3 shows the structure of the internal voltage controller. It is based on two Proportional Integral (PI) controllers, one for each of the dq channels, that introduce the internal states $x_{\rm dq}$. It expands upon the voltage controller studied in [14] by including additional Feed-Forward (FF) terms for current and voltage.

III. Preliminaries

This section presents some preliminary formulations that will be later used to assess the impact of the VI on the CF.

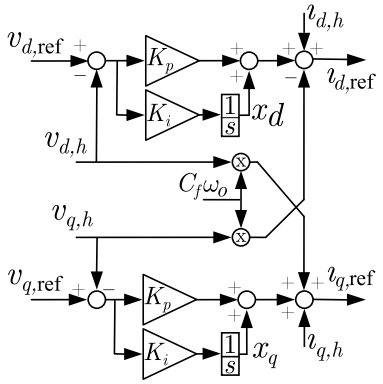

Fig. 3. Control scheme of an inner voltage controller with decoupling and feed-forward terms for current and voltage.

More information regarding CF and its application on the analysis of the control systems of power converters can be found in [5, 14]. A complex quantity $\overline{u}$ can be expressed in polar or rectangular form, as in:

$$\begin{aligned}\overline{u} &= u_d + \jmath\, u_q = u\exp(\jmath\varphi)\,,\\ &= \exp\big(\ln(u) + \jmath\varphi\big), \quad u \neq 0\,.\end{aligned} \tag{1}$$

where $u = \sqrt{u_d^2 + u_q^2}$ and $\varphi = \arctan(u_q/u_d)$. Taking the time derivative of (1) results in:

$$\dot{\overline{u}} = (\dot{u}/u + \jmath\dot{\varphi})\,\overline{u} = (\rho_u + \jmath\omega_u)\,\overline{u} = \overline{\eta}_u\,\overline{u}\,. \tag{2}$$

The quantity $\overline{\eta}_u$ has been defined in [5] as the CF of time-dependent Park vectors of the voltage and of the injected current at bus h, as follows:

$$\dot{\overline{v}}_h = \overline{\eta}_v\,\overline{v}_h\,, \qquad \dot{\overline{\imath}}_h = \overline{\eta}_\imath\,\overline{\imath}_h\,. \tag{3}$$

The CF includes a real and an imaginary part, with each one depending exclusively on the magnitude and phase angle of the Park vector, respectively. One should note that the use of CF as a derivative operator is general for any control signal, not limited only to voltages and currents [14]. It is noted also that, during transients, $\overline{\eta}_v \neq \overline{\eta}_\imath$ [5]. Using Park vectors, the instantaneous power injected at a bus h can be written as a complex quantity, as follows:

$$\overline{s}_h = \overline{v}_h\,\overline{\imath}_h^*\,, \tag{4}$$

where * denotes the complex conjugate operator. The rate of change of complex power is:

$$\begin{aligned}\dot{\overline{s}}_h &= \dot{\overline{v}}_h\,\overline{\imath}_h^* + \overline{v}_h\,\dot{\overline{\imath}}_h^*\\ &= \overline{\eta}_v\,\overline{v}_h\,\overline{\imath}_h^* + \overline{v}_h\,\overline{\eta}_\imath^*\,\overline{\imath}_h^*\\ &= (\overline{\eta}_v + \overline{\eta}_\imath^*)\,\overline{s}_h\,.\end{aligned} \tag{5}$$

The above equation will be used in the following section to derive the effect of the VI controller on the CF.

IV. Complex Frequency Derivations

A. Virtual Impedance Effect on Complex Frequency

The equation that describes the VI loop is [11]:

$$\overline{v}_{\rm ref} = \overline{v}_Q - \overline{Z}_v\overline{\imath}_h, \tag{6}$$

where $\overline{Z}_v = R_v + \jmath X_v$ is the virtual impedance and $\overline{v}_Q$ is the input of the VI, calculated from an outer voltage controller [10, 14]. By assuming ideal voltage control ($\overline{v}_{\rm ref} \approx \overline{v}_h$) and taking the derivative of (6), one derives:

$$\overline{\eta}_v \overline{v}_h = \overline{\eta}_{v_Q} \overline{v}_Q - \overline{Z}_v \overline{\eta}_\imath \bar{\imath}_h. \tag{7}$$

By assuming constant (or slowly changing) $\overline{v}_Q$, $\overline{\eta}_{v_Q} \overline{v}_Q = 0$ and thus, one derives:

$$\boxed{\overline{\eta}_v \overline{v}_h = -\overline{Z}_v \overline{\eta}_\imath \bar{\imath}_h.} \tag{8}$$

By multiplying both sides of (8) by $\bar{\imath}^*$, one derives:

$$\overline{\eta}_v \overline{v}_h \bar{\imath}_h^* = \overline{\eta}_v \bar{s}_h = -\overline{Z}_v \overline{\eta}_\imath \imath_h^2 = -\overline{\eta}_\imath \bar{s}_Z, \tag{9}$$

where $\bar{s}_Z$ is the power "consumed" by the virtual impedance. By solving (9) for $\overline{\eta}_\imath$ and then by applying the conjugate operator and substituting the result in (5), the contribution of the VI to the complex frequency of the voltage is derived:

$$\boxed{\dot{\bar{s}}_h = \overline{\eta}_v \bar{s}_h - \overline{\eta}_v^* \frac{s_h^2}{\overline{Z}_v^* \imath_h^2}.} \tag{10}$$

Equation (10) shows that the VI causes a "complex modulation" to the CF. This equation captures the specific contribution of the VI control to the bus frequency, something impossible to evaluate when using standard system formulations. Furthermore, this equation also assumes a non-zero value of $\overline{Z}_v$. If $\overline{Z}_v = 0$, the result is an ideal voltage controller. In that case, it can be concluded from (6) that : $\overline{v}_Q = \overline{v}_{\rm ref} \approx \overline{v}_h$ and thus, the frequency at the bus exclusively depends on the dynamics of the outer voltage controller.

B. Virtual Impedance with Voltage Controller

The equations of a PI-based, voltage controller (including FF) are [19]:

$$\begin{aligned} \dot{\overline{x}} &= \overline{v}_{\rm ref} - \overline{v}_h, \\ \bar{\imath}_{\rm ref} &= K_p(\overline{v}_{\rm ref} - \overline{v}_h) + K_i \overline{x} + \jmath C_f \omega_o \overline{v}_h + \bar{\imath}_h, \end{aligned} \tag{11}$$

where $\overline{x}$ is the internal state of the PI, K_p and K_i are the proportional and integral gains, respectively, and C_f is the capacitance of the LC filter. By applying Kirchhoff's current law to the output node of the LC filter (see Figure 1), the current injected in h is obtained as a function of the inductor current $\bar{\imath}_L$ and the capacitor current $\bar{\imath}_C$:

$$\bar{\imath}_h = \bar{\imath}_L - \bar{\imath}_C = \bar{\imath}_L - C_f \dot{\overline{v}}_h = \bar{\imath}_L - C_f \overline{\eta}_v \overline{v}_h. \tag{12}$$

By neglecting the electromagnetic transient effects of the capacitor ($C_f \overline{\eta}_v \overline{v}_h \approx C_f \jmath \omega_o \overline{v}_h$), assuming an ideal current controller ($\bar{\imath}_{\rm ref} \approx \bar{\imath}_L$) and substituting (6), (12), equation (11) becomes:

$$\begin{aligned} \dot{\overline{x}} &= \overline{v}_Q - \overline{Z}_v \bar{\imath}_h - \overline{v}_h, \\ 0 &= K_p(\overline{v}_Q - \overline{Z}_v \bar{\imath}_h - \overline{v}_h) + K_i \overline{x} \\ &= \overline{v}_Q - \overline{Z}_v \bar{\imath}_h - \overline{v}_h + \kappa_{\rm PI} \overline{x}, \end{aligned} \tag{13}$$

where $\kappa_{\rm PI} = K_i/K_p$. Equation (13) represents the dual expression of a current controller with decoupling and voltage FF, presented in [14], for a voltage controller. Through the cancellation of the opposite terms in (13), the dq-channel decoupling and the disturbance rejection capability of the controller is improved. By taking the derivative of the second equation of (13), the following is obtained:

$$(\overline{\eta}_v + \kappa_{\rm PI}) \overline{v}_h = (\overline{\eta}_{v_Q} + \kappa_{\rm PI}) \overline{v}_Q - (\overline{\eta}_\imath + \kappa_{\rm PI}) \overline{Z}_v \bar{\imath}_h. \tag{14}$$

One should note that (14) is a generalised form of (7) that takes into consideration the effect of the voltage controller. By multiplying both sides of the equation with $\bar{\imath}^*$, the above relation is expressed in terms of complex power:

$$\begin{aligned} &(\overline{\eta}_v + \kappa_{\rm PI}) \overline{v}_h \bar{\imath}^* = (\overline{\eta}_{v_Q} + \kappa_{\rm PI}) \overline{v}_Q \bar{\imath}^* - (\overline{\eta}_\imath + \kappa_{\rm PI}) \overline{Z}_v \imath_h^2, \\ \Rightarrow \quad &(\overline{\eta}_v + \kappa_{\rm PI}) \bar{s}_h = (\overline{\eta}_{v_Q} + \kappa_{\rm PI}) \bar{s}_Q - (\overline{\eta}_\imath + \kappa_{\rm PI}) \bar{s}_Z. \end{aligned} \tag{15}$$

By solving for $\overline{\eta}_\imath$, applying the conjugate operator and substituting in (5), the contribution of each separate controller to the CF of the voltage is analytically derived. This facilitates the understanding of the cascaded control structure and simplifies the controller gain selection.

TABLE I
HARDWARE AND CONTROL PARAMETERS FOR THE VSC.

Parameter	Value [pu]	Parameter	Value [pu]
C_f	0.01	L_f	0.08
P/f droop	1	Q/V droop	1
P/f T_s	0.001 s	Q/V T_s	0.001 s
K_p voltage	0.59	K_i voltage	10
K_p current	1.27	K_i current	14.3

V. SIMULATION RESULTS

To validate the theoretical developments, a case study considering a modified version of the well-known, WSCC 9-bus system is presented in this section. Compared to the standard system, a VSC-interfaced energy storage system is additionally connected at bus 5 of the network. It is shown in Figure 1 and modeled as in [20]. The grid-forming operation of the VSC is achieved through P/f and Q/V droop controllers as in [21, 22]. The dynamics of the LC filter and the inner voltage and current control loops are considered for the simulations. The control and hardware parameters that were used for the VSC are presented in Table I. The CF components ρ_v and ω_v are calculated as in [5]. The synchronous generators are modeled using standard fourth order models. All simulations were carried out with the Dome software tool [23]. The contingency that is used for all examples is a disconnection of the load at bus 5 at $t = 0.1$ s. The active power injection for the VSC was set to 0.7 pu for all cases. With the adopted current convention for the VSC, negative active power signifies power injection to the grid while positive reactive power signifies inductive operation. All frequencies in this section refer to deviations from the nominal values ($\rho_v = 0$ and $\omega_v = 1$ pu).

A. Effect of Virtual Resistance

Figure 4 shows the real and imaginary parts of the CF at bus 5 for different values of virtual resistance R_v. For these simulations, the value for the virtual reactance was set to $X_v = 0$. The value of R_v affects both components of the CF, as predicted by (10). Moreover, for higher values of R_v, the system damping improves and the system recuperates faster from the contingency. Figure 5 shows the active and reactive

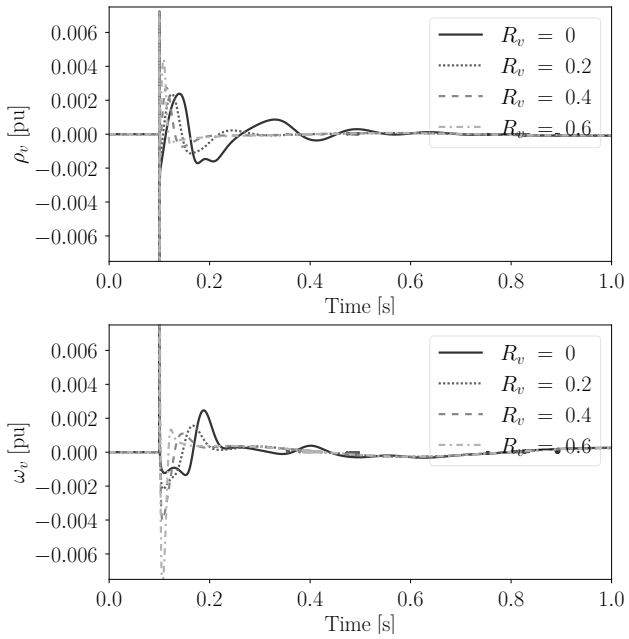

Fig. 4. Real (top) and imaginary (bottom) parts of the CF as seen at bus 5 of the WSCC 9-bus system during the disconnection at $t = 0.1$ s of the load at bus 5. Simulation for different values of virtual resistance R_v.

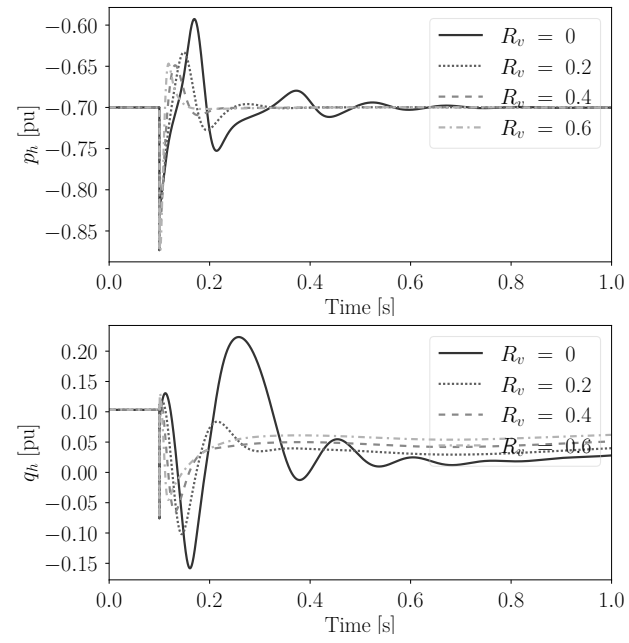

Fig. 5. Active (top) and reactive (bottom) power injected by the VSC at bus 5 of the WSCC 9-bus system during the disconnection at $t = 0.1$ s of the load at bus 5. Simulation for different values of virtual resistance R_v.

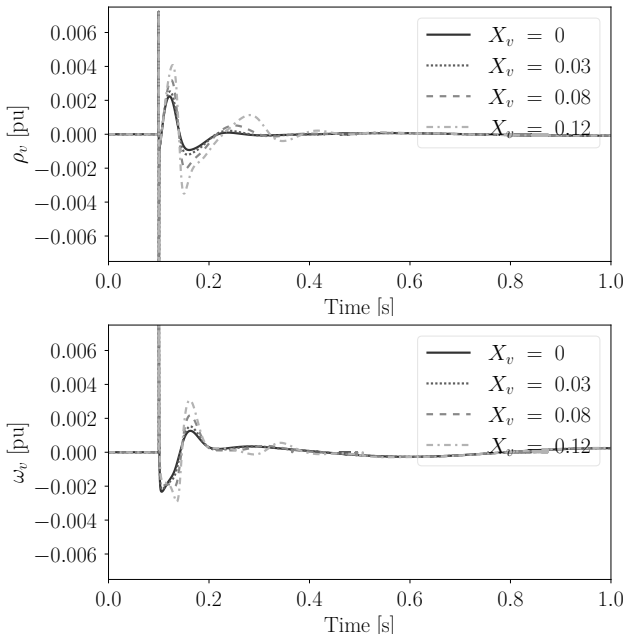

Fig. 6. Real (top) and imaginary (bottom) parts of the CF as seen at bus 5 of the WSCC 9-bus system during the disconnection at $t = 0.1$ s of the load at bus 5. Simulation for different values of virtual reactance X_v.

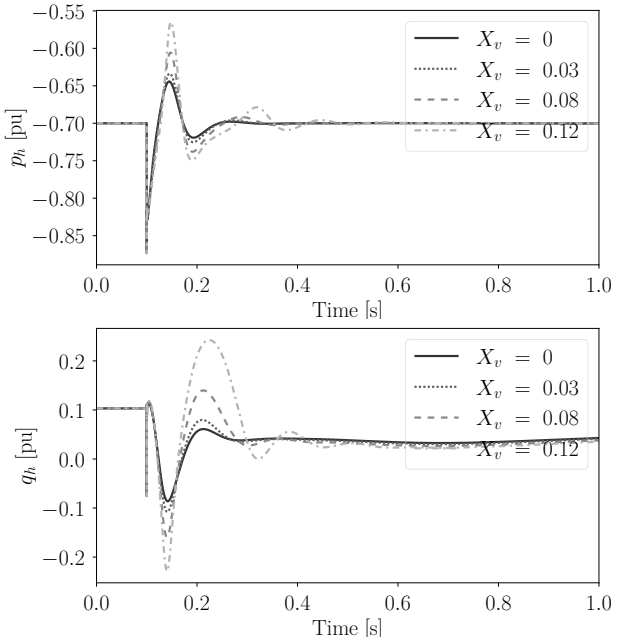

Fig. 7. Active (top) and reactive (bottom) power injected by the VSC at bus 5 of the WSCC 9-bus system during the disconnection at $t = 0.1$ s of the load at bus 5. Simulation for different values of virtual reactance X_v.

power injection of the VSC. It is confirmed that R_v has a stabilizing effect on the system, reducing the post-contingency oscillations. Lastly, the observed deviation in the steady-state values of q_h correspond to the power "consumed" by the virtual impedance, as noted in (9).

B. Effect of Virtual Reactance

Figure 6 shows the real and imaginary parts of the CF at bus 5 for different values of virtual reactance X_v. The value for the

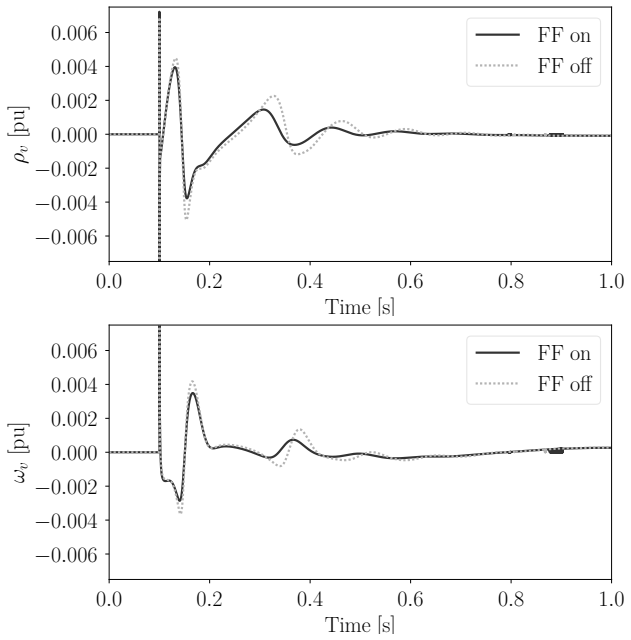

Fig. 8. Real (top) and imaginary (bottom) parts of the CF as seen at bus 5 of the WSCC 9-bus system during the disconnection at $t = 0.1$ s of the load at bus 5. Simulation with and without the FF applied to the voltage controller.

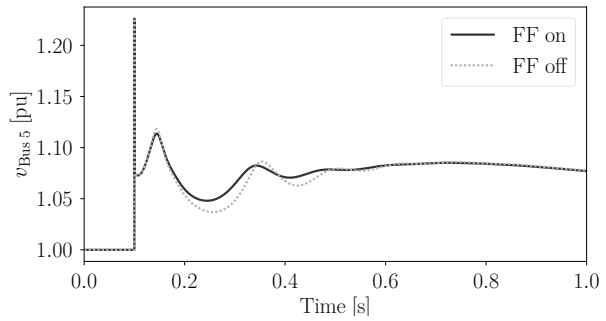

Fig. 9. Voltage magnitude at bus 5 of the WSCC 9-bus system during the disconnection at $t = 0.1$ s of the load at bus 5. Simulation with and without the FF applied to the voltage controller.

virtual resistance was set to $R_v = 0.25$. Similar to the previous case, the different values of X_v impact both components of the CF. However, higher values of X_v exacerbate the oscillations after the contingency. The difference in varying the VI through its real or imaginary part is accounted in (10). The use of CF allows studying the effect of the virtual reactance on frequency caused by the change of both voltage magnitude and phase angle. The selected parameter range for X_v was small because stability was lost for larger values. Figure 7 shows the active and reactive power delivered by the VSC, which confirms the deteriorating trend of the system state with the increase of X_v. It is concluded from this case that, while virtual reactance can improve the stability margin of multiple converters connected in parallel, it can have adverse effects on the transient operation of the VSC.

C. Effect of FFs

Figure 8 shows the complex frequency components while Figure 9 shows the voltage magnitude at bus 5. Initially, the full control diagram as shown in Figure 3 was used. Then, both the decoupling and current FF were disabled. The simulation results confirmed that the FF affects the transient response of the VSC, justifying their inclusion in the equations (11), (13). Furthermore, it is shown that the effect of the FF is beneficial for the operation of the system, slightly mitigating the oscillations that appear after the load disconnection. This is consistent with equation (13) that illustrates the benefits of the FF.

VI. Conclusion

In this paper, the concept of CF has been used to derive the analytical relation between the VI control parameters and the frequency at the connection bus of a grid-forming VSC. First, the effect of the VI on the CF at the connection bus has been calculated by simplifying the rest of the control system dynamics. Then, the expressions have been generalised to include the effects of the PI-based, cascaded voltage control and the decoupling and current FF. Theoretical results have been validated by using a case study based on a modified model of the WSCC 9-bus system. In the study, a set of recommended actions for the design of VI has been outlined.

Results show that the VI parameters affect the transient operation of the system through both the magnitude- and phase angle-dependent components of the CF. In particular, the system is shown to be robust against variations of the virtual resistance. Higher values of R_v, in fact, are shown to improve the system damping and, in general, its transient operation. On the other hand, higher values of the virtual reactance parameter X_v deteriorate the system transient response, increasing the magnitude of the frequency oscillations after a contingency. Finally, the decoupling and current FF are shown to improve the performance of the system by damping the frequency oscillations post-contingency. Future work will focus on the study of more complex implementations of the VI controller as well as on the impact on the CF of multiple grid-forming VSCs with VI operating in parallel.

References

[1] J. Sun, "Impedance-based stability criterion for grid-connected inverters," *IEEE Trans. on Power Electronics*, vol. 26, no. 11, pp. 3075–3078, 2011.

[2] X. Wang, Y. W. Li, F. Blaabjerg, and P. C. Loh, "Virtual-impedance-based control for voltage-source and current-source converters," *IEEE Trans. on Power Electronics*, vol. 30, no. 12, pp. 7019–7037, 2014.

[3] J. He and Y. W. Li, "Analysis, design, and implementation of virtual impedance for power electronics interfaced distributed generation," *IEEE Trans. on Ind. Apps.*, vol. 47, no. 6, pp. 2525–2538, 2011.

[4] A. Rodríguez-Cabero, J. Roldán-Pérez, and M. Prodanovic, "Virtual impedance design considerations for virtual synchronous machines in weak grids," *IEEE Journal of Emerging and Selected Topics in Power Electronics*, vol. 8, no. 2, pp. 1477–1489, 2019.

[5] F. Milano, "Complex frequency," *IEEE Trans. on Power Systems*, vol. 37, no. 2, pp. 1230–1240, 2022.

[6] J. M. Guerrero, J. Matas, L. G. de Vicuna, M. Castilla, and J. Miret, "Decentralized control for parallel operation of distributed generation inverters using resistive output impedance," *IEEE Trans. on Ind Electronics*, vol. 54, no. 2, pp. 994–1004, 2007.

[7] H. Wang, M. Han, R. Han, J. M. Guerrero, and J. C. Vásquez, "A decentralized current-sharing controller endows fast transient response to parallel dc–dc converters," *IEEE Trans. on Power Electronics*, vol. 33, no. 5, pp. 4362–4372, 2017.

[8] A. D. Paquette and D. M. Divan, "Virtual impedance current limiting for inverters in microgrids with synchronous generators," *IEEE Trans. on Ind. Apps.*, vol. 51, no. 2, pp. 1630–1638, 2014.

[9] F. Göthner, J. Roldán-Pérez, R. E. Torres-Olguin, and O.-M. Midtgård, "Harmonic virtual impedance design for optimal management of power quality in microgrids," *IEEE Trans. on Power Electronics*, vol. 36, no. 9, pp. 10 114–10 126, 2021.

[10] A. González-Cajigas, J. Roldán-Pérez, and E. J. Bueno, "Design and analysis of parallel-connected grid-forming virtual synchronous machines for island and grid-connected applications," *IEEE Trans. on Power Electronics*, vol. 37, no. 5, pp. 5107–5121, 2021.

[11] S. D'Arco, J. A. Suul, and O. B. Fosso, "A virtual synchronous machine implementation for distributed control of power converters in smartgrids," *Elec. Pow. Sys. Res.*, vol. 122, pp. 180–197, 2015.

[12] H. Kirkham, W. Dickerson, and A. Phadke, "Defining power system frequency," in *IEEE PES General Meeting*. IEEE, 2018, pp. 1–5.

[13] F. Milano and A. Ortega, "Frequency divider," *IEEE Trans. on Power Systems*, vol. 32, no. 2, pp. 1493–1501, 2016.

[14] D. Moutevelis, J. Roldán-Pérez, M. Prodanovic, and F. Milano, "Taxonomy of power converter control schemes based on the complex frequency concept," *arXiv preprint arXiv:2209.11107*, 2022.

[15] X. He, V. Häberle, and F. Dörfler, "Complex-frequency synchronization of converter-based power systems," *arXiv preprint arXiv:2208.13860*, 2022.

[16] X. He, V. Häberle, I. Subotić, and F. Dörfler, "Nonlinear stability of complex droop control in converter-based power systems," *IEEE Control Systems Letters*, 2023.

[17] F. Milano, "A geometrical interpretation of frequency," *IEEE Trans. on Power Systems*, vol. 37, no. 1, pp. 816–819, 2022.

[18] P. Rodríguez, I. Candela, C. Citro, J. Rocabert, and Á. Luna, "Control of grid-connected power converters based on a virtual admittance control loop," in *15th European Conference on Power Electronics and Applications*. IEEE, 2013, pp. 1–10.

[19] S. D'Arco and J. A. Suul, "Virtual synchronous machines—classification of implementations and analysis of equivalence to droop controllers for microgrids," in *2013 IEEE Grenoble Conference*. IEEE, 2013, pp. 1–7.

[20] Á. Ortega and F. Milano, "Generalized model of VSC-based energy storage systems for transient stability analysis," *IEEE Trans. on Power Systems*, vol. 31, no. 5, pp. 3369–3380, 2015.

[21] N. Pogaku, M. Prodanovic, and T. C. Green, "Modeling, analysis and testing of autonomous operation of an inverter-based microgrid," *IEEE Trans. on Power Electronics*, vol. 22, no. 2, pp. 613–625, 2007.

[22] D. P. Moran-Rio, J. Roldán-Pérez, M. Prodanović, and A. Garcia-Cerrada, "Influence of the phase-locked loop on the design of microgrids formed by diesel generators and grid-forming converters," *IEEE Trans. on Power Electronics*, vol. 37, no. 5, pp. 5122–5137, 2021.

[23] F. Milano, "A Python-based software tool for power system analysis," in *IEEE PES General Meeting*. IEEE, 2013, pp. 1–5.